10-1-2002

ANG II AT(1) and AT(2) receptors in developing kidney of normal microswine

Susan P. Bagby
Oregon Health and Science University and Portland Veterans Affairs Medical Center

Linda S. LeBard
Oregon Health and Science University and Portland Veterans Affairs Medical Center

Zaiming Luo
Oregon Health and Science University and Portland Veterans Affairs Medical Center

Bryan E. Ogden
Oregon Health and Science University and Portland Veterans Affairs Medical Center

Christopher Corless
Oregon Health and Science University and Portland Veterans Affairs Medical Center

See next page for additional authors

AJP-Renal Articles in PresS. Published on May 22, 2002 as DOI 10.1152/ajprenal.00313.2001

AngII AT1 and AT2 Receptors in Developing Kidney of Normal Microswine

Susan P. Bagby, MD[1], Linda S. LeBard, BS[1], Zaiming Luo, MD[1], Bryan E. Ogden, DVM[2], Christopher Corless, MD/PhD[3], Elizabeth D. McPherson, BS[1], Robert C. Speth, PhD[4]

Departments of Medicine[1], Comparative Medicine[2], and Pathology[3]

Oregon Health & Science University and Portland VA Medical Center, Portland, Oregon

And

Department of Veterinary and Comparative Anatomy[4], Pharmacology and Physiology[4],

School of Veterinary Medicine, Washington State University, Pullman, WA

Address correspondence to: Susan P. Bagby, MD

Professor of Medicine

Division of Nephrology

Oregon Health & Science University

3314 SW U.S.Veterans Hospital Rd, Suite 262

Portland, OR 97201-2940

Fax: 503-721-7810 email: bagbys@ohsu.edu

Key Words: AngII, developing kidney, AT1, AT2, quantitative autoradiography, swine

Abstract Word Count: 166

Abstract

To identify an appropriate model of human renin-angiotensin system (RAS) involvement in fetal origins of adult disease, we quantitated renal AngII receptors in fetal (GD 90, n=14), neonatal (3-wk, n=5), and adult (6-mo, n=8) microswine by autoradiography (^{125}I-Sar^{1}Ile^{8}AngII + cold CGP 42112 for AT1R, ^{125}I-CGP 42112 for AT2R) and by whole-kidney radioligand binding. Renal AT1R exhibited 10-fold increase postnatally ($p<.001$) with maximal postnatal density in glomeruli and lower-density AT1R in extra-glomerular cortex and outer medulla. Cortical levels of AT2R by autoradiography fell with age from $\cong$ 5000 fmol/g in fetal kidneys to $\cong$ 60% and 20% of fetal levels in neonatal and adult cortex respectively ($p<.0001$). Swine renal AT2R binding mimicked that described in primate - but not rodent - species: dense AT2R confined to discrete cortical structures which included pre- and juxta- (but not intra-) glomerular vasculature. Results provide a quantitative assessment of AngII receptors in developing pig kidney and document concordance of pig and primate in developmental regulation of renal AT1 and AT2 receptors.

KEY WORDS: renal development, AngII receptors, AT1R, AT2R, pig kidney, quantitative autoradiography, image analysis, radioligand binding

Introduction

The renin-angiotensin system (RAS) plays an important role in development of renal vascular and tubular structures[1,2]. Although ureteral bud induction during early nephrogenesis occurs in *in vitro* organ culture despite angiotensin (AngII) AT1 receptor (AT1R) blockade[2], the in vivo role of AngII in determining nephron number remains controversial. Emerging evidence also implicates the AngII AT2 receptor (AT2R) in renal development[3], both in morphogenesis of the urogenital system[4] and in fetal vasculogenesis and vascular differentiation[5].

Renal AT1 and AT2 receptors also play critical roles in postnatal renal hemodynamics and renal tubular function in both physiologic and pathologic states. Thus, AT1R stimulation promotes vasoconstriction and Na retention in the normal kidney and activates cellular growth and fibrosis in inflammatory disease states[1]. New evidence supports an active role of the AT2R in attenuation of renal AT1R responses[6], via AT2R activation of nitric oxide- and bradykinin-mediated vasodilation[7-9], pressure natriuresis[10], growth inhibition/apoptosis[11], and anti-fibrotic actions[12]. These actions underscore the importance of a balance between AT1R and AT2R activities in determining net in vivo renovascular response to AngII and thus vulnerability to hypertension when AT1R actions are unopposed[9].

Much of our information about AT1 and AT2 receptors derives from rodent models. Yet studies suggest potentially important differences between human and rodent in the

distribution of intrarenal AT2R[13]. Autoradiographic study of renal AngII receptors in rodents demonstrated absence of vascular AT2R[14,15], whereas similar human and simian studies reveal the consistent presence of AT2R in preglomerular arterioles[13,16-18]. To identify a non-primate animal model optimal for study of human RAS involvement in intrauterine growth retardation and the associated adult hypertension, we have examined AngII receptors in microswine, a species with cardiovascular, renal, and immune systems uniquely similar to the human[19,20]. We have quantitatively assessed renal AT1R and AT2R in normal fetal, neonatal, and adult microswine by autoradiography and membrane radioligand binding. Results indicate striking developmental differences in renal AT1R and AT2R density and/or distribution, document the histologic structures responsible for AT1/AT2 receptor binding, and emphasize the similar prominence of AT2R in postnatal preglomerular vasculature of porcine and human kidneys.

METHODS

Animal/Tissue Preparation: Time-bred normal microswine were obtained from Charles River Laboratories and maintained in the OHSU Animal Care Facility until study according to institutionally approved protocols (#A439). For fetal studies, sows at 90 days gestation underwent sterile Caesarian section, sequential fetal removal, and then euthanasia with 85 mg/kg Beuthanasia-D (Schering) IV. Each piglet was immediately sacrificed and the kidneys removed, length and weight recorded, and the tissue immediately immersed in ice-cold Phosphate Buffered Saline (PBS). 3-wk and 6-mo pigs under isofluorane anesthesia underwent a midline thoraco-abdominal incision for kidney removal. Coronal slices from the mid-right kidney were kept in ice-cold PBS for

3-4 hrs prior to processing for frozen sections. From each left kidney, tissue was placed in ice-cold PBS for membrane binding or snap-frozen in liquid nitrogen for RNA extraction. Additional renal tissue sections were quickly distributed to zinc-formalin (10%), Carnoy's solution, or fresh 4% paraformaldehyde for histology. Neonatal and adult (but not fetal) animals included in this report represent partial commonality with control pigs used in studies of intrauterine growth retardation (3-wk pigs: ID#s 2745, 2746, 2748, 2749, 2750; 6-mo adult pigs: ID#s 1285, 1286, 1153, 1155).

Film Autoradiography for AngII Receptors: Autoradiography for both AT1R and AT2R was performed within 24 hrs of tissue harvest based on preliminary observations that AT1R – but not AT2R – binding declines in storage (SBagby, unpublished, and reported studies [21]). Tissue blocks were snap-frozen in OCT® using a pentane-dry ice slurry; on the day of harvest, sequential 20 μm frozen sections were cut, placed on gelatin-coated slides, and kept at -80° C until study. On the following day, sections were thawed and pre-incubated for 30 min at room temperature in isotonic buffer [150 mM NaCl, 50 mM Tris, 50 μM Plummer's inhibitor (carboxypeptidase inhibitor), 20 μM bestatin (aminopeptidase inhibitor), 5 mM EDTA, 1.5 mM 1,10-phenanthroline, and 0.1% heat-treated protease-free BSA, pH 7.4]. Consecutive sections were incubated for 25 min in one of 4 isotonic-buffer solutions: 0.4 nM ^{125}I-Sar^{1}Ile^{8} Angiotensin II (*SIAII) for total AngII receptor binding; 0.4 nM *SIAII plus 10^{-6} M Sar^{1}AngII (nonselective analog) for nonspecific binding; 0.4 nM *SIAII plus 10^{-6} M Valsartan (Val, an AT1-selective antagonist) to demonstrate AT2R; and ; 0.4 nM *SIAII plus 10^{-6} M CGP 42112 (an AT2R selective compound) to demonstrate AT1R. To independently confirm AT2R

binding, we exposed a second set of 4 consecutive sections to: 0.4 nM ^{125}I-CGP 42112 (*CGP) for total binding; *CGP+ Sar^{1}AngII for nonspecific binding; *CGP+Val to confirm absence of AT1R binding, and *CGP+PD123319 (a chemically distinct AT2R selective compound) to confirm AT2R specificity of CGP 42112 in microswine. (Radioligands were purchased from Peptide Radioiodination Service Center, Washington State University, Pullman WA.) Sections were rinsed, dried, placed on Kodak Biomax MR1 xray film, and maintained at -80° C for 24 hrs. A standard slide with calibrated concentrations ranging from 1 to 600 nCi/mg ^{125}I (Microscales, Amersham-Pharmacia Biotech, Piscataway, NJ) was included in each cassette. Film was developed using an automated Kodak film processor.

Image Analysis: Images were captured using an AIS image analysis system (Imaging Research Inc, Ontario Canada) via analog camera. Average density of AngII receptors was determined by reference to the ^{125}I standards for each film. Because AT1R binding in fetal kidneys was low and diffusely distributed, average density was assessed across the whole-kidney area. In postnatal kidneys, using a threshold setting, AT1R binding was analyzed for size, for number/area, and for fractional area of cortex occupied by the distinctly denser glomerular profiles (identity confirmed, see below). AT1R density was assessed both within glomeruli and separately in the extraglomerular tissue. Fetal AT2R density was individually assessed in pelvic wall (“pelvis”), papilla, outer medulla, main cortex (excluding outer rim), and in subcapsular cortex. In postnatal cortical areas, where the AT2R occupied only a portion of the cross-sectional area, a threshold setting was used to assess the average AT2R density, size, and number/unit area of AT2R-rich

"Hotspots" and to also estimate the fraction (%) of the cortical cross-sectional area occupied by AT2R. Specific AT2R binding in intervening cortical tissue was undetectable in both neonatal and adult kidneys. Results for AT2R using *SIAII+Val were qualitatively similar but of lower resolution than those using *CGP 42112. Thus, formal analysis was restricted to *SIAII+CGP 42112 for quantitating AT1R and *CGP 42112 for AT2R, each with subtraction of the relevant non-specific binding density. Image analysis data for each receptor subtype were analyzed by ANOVA, either one-way with age as the experimental factor or, if data permitted, 2-way with age and region of kidney as factors. Sex-related differences were evaluable only in fetal kidney.
To identify histologic sites of ATR binding, adjacent frozen sections were processed for autoradiography or immunostained by an avidin-biotin protocol previously detailed [22] for Factor-VIII related antigen (Dako Corp, 1:4000 dilution). Slide images were digitized, identically sized, and electronically overlaid.

AngII Receptor Binding in Fresh Kidney Membranes: Freshly harvested tissue from 14 fetal and 8 adults animals was processed according to standard methods, including homogenization, preparation of a crude membrane fraction via 100,000 x g ultracentrifigation, protein assay (Biorad), and incubation of 20-100 μg protein/well at 37°C with appropriate radioligands in 150 ul assay volume. Each binding assay included: *SIAII and *CGP saturation curves (each in triplicate) and *SIAII displacement curves using CGP 42112 (displacement), Valsartan (AT1R displacement), or AngII (AT1R and AT2R displacement), each done in duplicate with a nonspecific-binding well. Average specific binding was calculated in Excel (Microsoft Inc, Redmond WA) as fmol

radioligand/mg lysate protein); curves were analyzed in PRISM (GraphPad Software, San Diego, CA) and statistical analysis carried out using SigmaStat (Jandel Scientific Software, San Rafael, CA) via ANOVA for effects of age (fetal vs adult) or sex (fetal data only) on: 1) maximum binding (Bmax) for *SIAII (AT1R + AT2R), for *CGP (AT2R), and for AT1R by difference; 2) Kd for each radioligand; 3) % AT1R using valsartan displacement curves; % AT2R using CGP 42112 displacement curves; and log IC_{50} for each displacing AngII analog by standard PRISM formulas.

Results

AT2 RECEPTORS

FETAL KIDNEY. By autoradiography, AT2R were overwhelmingly predominant in fetal kidney (**FIGs 1, 2**), maximally dense in primordial papillary regions ($p<.025$ vs other areas) and extending in spoke-like cords to a distinct outer nephrogenic region. Despite trends toward higher AT2R density in several regions of female kidneys (**FIG 2**), there were no significant sex differences in autoradiographic AT2R density. By radioligand binding (**Table 1**, **FIG 3**), fetal kidney again exhibited high levels of total AngII receptors (combined average 352 ± 276 fmol/mg protein, n=14) which were $96 \pm 3\%$ AT2R by competition binding and by comparing *SIAngII Bmax (total ATR) vs *CGP Bmax (AT2R only) (**Table 1**). As in autoradiographic AT2R binding, there were no significant sex differences in receptor number (Bmax) or subtype distribution. However, Kd for both *SIAII and *CGP 42112 were significantly higher in females than in males (**Table 1**), indicating a lower AT2R affinity in the fetal female kidney. (Because of the predominance of AT2R, *SIAII binding affinity in this context also reflects primarily that

of the AT2R). Because differing Kd values could bias results of autoradiographic receptor density, we reexamined the effect of sex on AT2R density after adjustment for the sex-dependent Kd differences. However, even after this adjustment, AT2R density values did not differ significantly between fetal males and females.

.

NEONATAL KIDNEY. By comparison with fetal kidney, 3-wk neonatal kidney (**FIG 4**) exhibited a lower density of cortical AT2R by autoradiography (**FIG 5** vs **FIG 2**) (p=.002 vs fetal,) and a substantially altered distribution pattern (**FIG 4** vs **FIG1**). Thus, AT2R binding in neonatal cortex was confined to discrete AT2R-rich clusters (AT2R "Hotspots") with no detectable specific binding in the intervening cortical tissue (**FIG 5**). Average AT2R density within neonatal Hotspots in both subcapsular and main cortex significantly exceeded the density of the linear outer medullary and the low diffuse papillary AT2R (**FIG 5**: regional difference p<.001). Intense pelvic-wall AT2R binding was similar to cortical Hotspot levels. AT2R Hotspots in the subcapsular cortex occupied a higher fractional area (p<.025) and were more numerous per unit area (p<.01) than those of the main cortex (**FIG 6**). AT2R Hotspot size did not differ between the two cortical regions. The AT2R-dense structures were often linear and sometimes branching. Based on overlays of autoradiographic and adjacent histologic images immunostained for Factor VIII-related antigen (**FIG 7,** lefthand panels), AT2R Hotspots included some (but not all) vessels (specifically small intra-cortical arterioles and microvessels of the outer medulla), juxta- (but not intra-) glomerular structures, and large neural trunks accompanying penetrating pelvic vessels. [Note: Attempted radioligand binding using both *SIAII and *CGP in neonatal whole-kidney homogenates

yielded barely detectable binding in only 2 of 8 neonatal kidneys tested (data not shown)].

ADULT KIDNEY. In adult kidney cortex, AT2R similarly exhibited a “starry-sky” distribution pattern: discrete clusters of intense AT2R binding with no detectable binding in the intervening tissue (**FIGs 8, 9**). Unlike neonates, there was no distinct subcapsular region in *CGP autoradiographs of adult kidneys. Average AT2R density of adult cortical Hotspots (**FIG 9**) was ≅ 15% that of fetal cortex and ≅ 25% that of neonatal Hotspots (**Table 2**; age effect: p<.0001). As in neonates, selected adult autoradiographs demonstrated AT2R binding in larger renal vessels (eg **FIG 8**). As compared to neonatal Hot Spots, adult AT2R Hotspots were larger in size (p=.05) but fewer per unit area (p<.01), thus occupying a comparable fractional area of cortex (**Table 2**). Using overlays of autoradiographic vs histologic images from adult kidney sections as described for neonates, AT2R-positive structures were again found to include small intra-cortical arterioles and juxta-glomerular sites, while the main glomerular tufts were consistently negative for AT2R binding (not shown). Although not present with enough consistency in autoradiographic sections for statistical analysis, adult pelvic wall typically exhibited intense AT2R binding. In contrast, unlike neonatal kidney, there was no detectable AT2R in adult medulla (**FIG 8**).

By radioligand binding in adult kidney membranes, total Ang II receptors were low, detectable in only 4 of 8 kidneys studied and averaging ≅ 1% of fetal total ATR levels. *SIAII Bmax in the 4 adult kidneys averaged 5 ± 3 fmol/mg protein, of which 0-30%

were AT2R. Representative binding curves are shown in **FIG 10**. However, AT2R as assessed by *CGP saturation binding were undetectable in all 8 adult kidneys. Of potential importance, the insensitivity of *CGP – despite its high affinity for AT2R – may be due to the unusually high nonspecific binding in renal membranes, this despite the remarkably low nonspecific binding in renal autoradiographs. Separating cortex vs medulla in binding assays did not improve the sensitivity of radioligand binding in adult pig kidneys (data not shown). Thus, as in neonates, radioligand binding in whole-kidney adult porcine membranes were insufficiently sensitive to consistently quantitate AngII receptor status.

AT1 RECEPTORS

FETAL KIDNEY. By autoradiography, AT1R binding in fetal kidney was very low but consistently detectable, distributed diffusely throughout the cortex while absent in primordial papilla (**FIG 1,** lower right panel). AT1R density in fetal kidney was $\cong 1/40^{th}$ that of fetal AT2R (**FIG 2:** note separate Y axis scale for AT1R vs AT2R). There were no AT1R-dense structures in fetal cortex comparable to the glomerular profiles present in postnatal kidneys. Although AT1Rs were difficult to directly detect by competition binding due to the large excess of AT2R, comparison of *SIAII (total) vs *CGP (AT2R only) binding in kidney membranes yielded an estimate of 4 $\pm$ 3% AT1R, which were also detectable by *SIAII saturation binding carried out in the presence of AT2R blockade with 1 μM *CGP42112 **(Table 1; FIG 3D).**

NEONATAL KIDNEY. The pattern of AT1R distribution in 3-Wk neonatal cortex tissue (**FIG 4**, lower right panel) was one of AT1R-dense glomerular profiles, seen as uniformly round “dots”, superimposed on diffuse, less-dense AT1R binding in the intervening cortical tissue. AT1R density of neonatal glomerular profiles was 10-fold higher than that of fetal cortex, was comparable in the glomerular profiles of subcapsular and main cortex regions, and was significantly higher than that in the extraglomerular cortex or medullary tissue (**FIG 5**). However, neonatal subcapsular vs main cortex areas exhibited significant differences in binding patterns: AT1R-dense glomerular profiles occupied a >10-fold larger fraction of the subcapsular area than of the main cortex area ($p<.001$; **FIG 6**). Also, average size of the glomerular profiles by image analysis was ≅ 4-fold increased in the subcapsular vs main cortex. However, this apparently increased size of neonatal subcapsular > main-cortex glomeruli was not supported by histologic assessment (**FIG 7**, right-hand panel). Instead, normal-sized, Factor VIII-antigen-positive glomeruli in the subcapsular cortex were densely packed along with less mature glomeruli, which lacked Factor VIII-antigen immunoreactivity but did exhibit AT1R binding (**FIG 7**). This high density of subcapsular glomeruli caused overlapping outlines of adjacent glomerular profiles during use of the threshold setting for image analysis, overestimating glomerular size while underestimating #/unit area. Thus, it is the increased number of glomeruli/unit area and the concomitant increase in fractional area occupied by glomerular profiles (but not the size of glomeruli) that distinguishes subcapsular (nephrogenic) from main cortex. (Overlapping of glomerular profiles was not an issue in the main cortex of neonates nor in adult kidney cortex.)

In adult kidney, there was, as for AT2Rs, no distinguishable subcapsular cortical region in AT1R autoradiographs (**FIG 8**). Concordance of AT1R-rich "hotdots" and glomerular profiles in adult kidney was confirmed as described for neonatal kidney (not shown). Average AT1R density of adult glomerular profiles was significantly higher than that of extraglomerular cortical and outer medullary areas (**FIG 9**; $p<.025$) and was comparable to that of neonatal glomeruli (p NS)(**Table 2**). The average size (cross-sectional area) of AT1R-dense adult glomerular profiles were > 3-fold larger than that of the glomerular profiles in the main cortex of neonates ($p=.001$). Adult glomerular profiles occupied $10 \pm 5\%$ of cortical area, as compared to $3 \pm 2\%$ of the main cortex area in neonates ($p=.03$)(**Table 2**). The number of glomerular profiles per unit area did not differ between adult cortex and neonatal main-cortex (**Table 2**).

Discussion

We have examined the distribution and densities of AT1 and AT2 Angiotensin II receptor binding in the normal kidneys of developing microswine, a species with renal anatomy and physiology uniquely similar to that of the human kidney[20]. Our major findings include: 1) reciprocal developmental changes in AT1R (increasing) and AT2R (decreasing) density in microswine kidney from gestation Day 90 (of 115) to post-pubertal adulthood; 2) identification and quantitation of distinct postnatal regional distribution patterns for AT1R (maximally dense in glomeruli with diffuse extra-glomerular cortical and outer medullary binding) vs AT2R (confined to pre- and juxta-glomerular arterioles, outer medullary microvessels, and some neural elements) in swine renal tissue; 3) sex differences in AT2R binding affinity in fetal kidney; and 5)

similarity of porcine and human kidneys in the prominent presence and distribution pattern of AT2R[17,18].

We are unable to identify prior reports of renal AngII receptors in swine. Grone et al reported that virtually 100% of AngII receptors in human fetal kidney are AT2R[16], in agreement with our findings in fetal pig kidney. ATR binding in the postnatal human kidney by autoradiography has been described in 4 studies: 3 of 4 reported predominant AT2Rs in preglomerular arteries in an adventitial location[13,17,18,23]; glomeruli and outer medullary vascular bundles exhibited dense AT1Rs, tubules showed less dense AT1Rs. Similarly, in simian kidney, AT2R were dominant in arteries, while glomeruli contained only AT1R and the JG apparatus exhibited both subtypes[13]. One report which failed to find AT2R in human intra-renal vasculature[24] was based on limited human material. An immunochemistry study in human kidneys reported mild-moderate immunoreactive AT2R protein in blood vessels, together with weak staining in glomeruli[25].

Overall, our autoradiographic findings in fetal and postnatal porcine kidney closely match these prior reports in primate kidneys. Our finding that AT1-rich “hotdots” represent glomerular profiles in pig conforms to results in other species using emulsion autoradiography [13,17,18,23]. Overlays of our autoradiographic and histologic images of pig kidney indicate that postnatal porcine glomeruli exhibit little if any AT2R, while cortical arterioles and outer medullary microvessels show dense AT2R binding. Our results do not indicate whether small-arteriole-associated AT2R reflects binding by medial wall, adventitia, and/or associated micro-neural elements. Comparison of extra-cortical

neonatal vs adult pig kidneys demonstrates loss or marked reduction of AT2R binding in medullary microvessels with aging, whereas the pelvic wall retains dense AT2R binding in adults. Finally, based on the diffuse and homogenous specific AT1R binding in the extra-glomerular cortical tissue, our results indicate that the diverse tubular and vascular elements within this compartment contain AT1R at comparable densities.

The primate/porcine pattern of AT2R stands in distinct contrast to reports of AT1R/AT2R distribution in the rodent kidney. In a paired autoradiographic study of adult human and rat kidney, Gibson et al [13] found AT2Rs in human renal vasculature but no AT2R in rat kidney. Song et al also found only AT1R in adult rat renal structures[14]. Immunochemical studies of rat kidney by Ozono et al[15], using a well-validated anti-AT2R antibody, demonstrated virtual disappearance of AT2R protein by 4 wks of age, whereas low Na diet induced reappearance of AT2R protein. This was localized to glomerular and interstitial sites, not to vasculature sites[15]. In disagreement with these reports, Miyata et al found immunoreactive AT2R protein thoughout the rat kidney except in glomerulus and thick ascending limb[26]. Finally, Cao et al[27] applied radioiodinated CGP-42112 autoradiography to rat kidney sections and found extensive AT2R binding, most prominent in the inner cortex. This did not, however, reproduce the pattern reported in primate and porcine kidney (as described above). Studies of AT2R mRNA in rat kidney are also discrepant. Norwood et al[16] found no AT2R mRNA in 1-mo-old rat kidney and Kakuchi et al[28] noted disappearance of rat renal AT2R mRNA at birth. However, Miyata et al reported positive AT2R mRNA in all rat renal compartments except glomeruli and medullary thick ascending limb[26].

Because we were unable to reconcile these differences in reported studies of AT2R binding and mRNA in postnatal rodent kidney, we examined AT1R and AT2R in 3 normal adult rat kidneys by autoradiographic techniques identical to those used in our adult microswine. Confirming the results of Gibson et al [13], no specific AT2R binding was detectable in adult rat kidney after 24 hrs exposure (**FIG 11**). This does not exclude AT2R in rat kidney; macrovascular AT2R in pig require 3-4 weeks exposure for detection. However, the differences noted demonstrate a substantially lower AT2R density in adult rat kidney as compared to adult porcine kidney.

Previous reports of vascular AT2R in primate kidney localize the receptors to the adventitial layer[13,17]. We have recently examined localization of AngII ATRs in conduit arteries (including the main renal artery) in normal microswine (SBagby et al, submitted). We found that AT2Rs localize to a discrete circumferential cell layer along the medial-adventitial border in what would typically be described as adventitia. However, using smooth-muscle-specific alpha (α) actin immunochemistry in parallel with AT2R autoradiography, AT2R-positive cells, while α actin-negative, in fact extend into the outermost medial layer, occupying what Stenmark et al have described as "intersititial spaces" lying between longitudinal muscle bundles[29,30]. These medial-adventitial boundary cells, which formed a continuous layer extending from abdominal aorta into its branch-artery walls, are optimally positioned to mediate AT2R-dependent effects of AngII generated locally in vascular interstitium[31,32]. Recent studies support an active role for AT2Rs in both modulating renovascular responses to AngII and

regulating systemic blood pressure. Thus, in vivo infusion of AT2R-antisense oligonucleotide into the renal interstitial space in normal rats induced hypertension and enhanced pressor sensitivity to exogenous AngII[9], indicating a tonically active role of AT2R in the renal vasculature even in the rodent. Accordingly, the abundance of preglomerular arterial AT2Rs may well determine not only the renal hemodynamic response to AngII, but also the set point of renal homeostatic regulation of blood pressure.

Our studies raise questions about potential male-female differences in the AT2R, which is located on the X chromosome[33]. In radioligand binding studies of fetal kidneys, female membranes exhibited significantly lower affinity (higher Kd) for both *CGP and *SIAII radioligands. In autoradiographic studies, fetal female kidneys showed higher average density of AT2R in cortical and outer medullary regions, although this was not significant, even after adjusting for observed Kd differences. Unfortunately, our small numbers and serendipitous male/female distribution did not permit formal assessment of sex differences in either neonatal or adult animals.

In summary, we have demonstrated that developmental regulation of AngII receptors in microswine follows directional changes similar to those reported for other species: increasing AT1R and decreasing AT2R densities with aging. Further, AT1R density and distribution over the course of postnatal development is similar to that reported in both rodent and primate kidneys. In contrast, AT2Rs in postnatal pig kidney localize predominantly to cortical pre-glomerular and juxta-glomerular vasculature (and, in

neonates, to outer medullary vasculature), thus following a primate rather than a rodent pattern of renal AT2R distribution. Importantly, our results do not differentiate which vascular-wall components exhibit AT2R binding. Our findings provide new information on developmental AT1R and AT2R regulation in the pig kidney, support potentially important species differences in AngII AT2R receptor abundance and distribution, and validate the swine model for study of the renal RAS in fetal origins of human disease.

Acknowledgments

Work reported was funded by NIH/NICHHD grant # PO1 HD34430. The authors gratefully acknowledge the valued contributions of Vicki Feldmann, OHSU Laboratory Animal Technician; the outstanding support and skilled technical contributions of Carolyn Gendron and Linda Jauron-Mills of OHSU Heart Research Center Imaging Core Laboratory; the technical skills of photographer Michael Moody of the Portland VAMC Medical Media Service, and the administrative assistance of Kathleen Beebe in preparation of the manuscript.

References

1. Oliverio MI, Coffman TM. Angiotensin II Receptor Physiology Using Gene Targeting. *News Physiol Sci* 2000;15:171-175.

2. Alcorn D, McCausland JE, Maric C. Angiotensin receptors and development: the kidney. *Clin Exp Pharmacol Physiol Suppl* 1996;3:S88-S92.

3. Gallinat S, Busche S, Raizada MK, Sumners C. The angiotensin II type 2 receptor: an enigma with multiple variations. *Am J Physiol Endocrinol Metab* 2000;278:E357-E374.

4. Curhan GC, Chertow GM, Willett WC, Spiegelman D, Colditz GA, Manson JE, Speizer FE, Stampfer MJ. Birth weight and adult hypertension and obesity in women. *Circ* 1996;94:1310-1315.

5. Yamada H, Akishita M, Ito M, Tamura K, Daviet L, Lehtonen JY, Dzau VJ, Horiuchi M. AT2 receptor and vascular smooth muscle cell differentiation in vascular development. *Hypertension* 1999;33:1414-1419.

6. Ichiki T, Labosky PA, Shiota C, Okuyama S, Imagawa Y, Fogo A, Niimura F, Ichikawa I, Hogan BL, Inagami T. Effects on blood pressure and exploratory behaviour of mice lacking angiotensin II type-2 receptor. *Nature* 1995;377:748-750.

7. Dimitropoulou C, White RE, Fuchs L, Zhang H, Catravas JD, Carrier GO. Angiotensin II Relaxes Microvessels Via the AT(2) Receptor and Ca(2+)-Activated K(+) (BK(Ca)) Channels. *Hypertension* 2001;37:301-307.

8. Carey RM, Jin X, Wang Z, Siragy HM. Nitric oxide: a physiological mediator of the type 2 (AT2) angiotensin receptor. *Acta Physiol Scand* 2000;168:65-71.

9. Moore AF, Heiderstadt NT, Huang E, Howell NL, Wang ZQ, Siragy HM, Carey RM. Selective inhibition of the renal angiotensin type 2 receptor increases blood pressure in conscious rats. *Hypertension* 2001;37:1285-1291.

10. Liu KL, Lo M, Grouzmann E, Mutter M, Sassard J. The subtype 2 of angiotensin II receptors and pressure-natriuresis in adult rat kidneys. *Br J Pharmacol* 1999;126:826-832.

11. Yamada T, Horiuchi M, Dzau VJ. Angiotensin II type 2 receptor mediates programmed cell death. *Proc Natl Acad Sci USA* 1996;93:156-160.

12. Morrissey JJ, Klahr S. Effect of AT2 receptor blockade on the pathogenesis of renal fibrosis. *Am J Physiol* 1999;276:F39-F45.

13. Gibson RE, Thorpe HH, Cartwright ME, Frank JD, Schorn TW, Bunting PB, Siegl PK. Angiotensin II receptor subtypes in renal cortex of rats and rhesus monkeys. *Am J Physiol* 1991;261:F512-F518.

14. Song K, Zhuo J, Allen AM, Paxinos G, Mendelsohn FA. Angiotensin II receptor subtypes in rat brain and peripheral tissues. *Cardiology* 1991;79 Suppl 1:45-54.

15. Ozono R, Wang ZQ, Moore AF, Inagami T, Siragy HM, Carey RM. Expression of the subtype 2 angiotensin (AT2) receptor protein in rat kidney. *Hypertension* 1997;30:1238-1246.

16. Norwood VF, Craig MR, Harris JM, Gomez RA. Differential expression of angiotensin II receptors during early renal morphogenesis. *Am J Physiol* 1997;272:R662-R668.

17. Zhuo J, Dean R, MacGregor D, Alcorn D, Mendelsohn FA. Presence of angiotensin II AT2 receptor binding sites in the adventitia of human kidney vasculature. *Clin Exp Pharmacol Physiol Suppl* 1996;3:S147-S154.

18. Goldfarb DA, Diz DI, Tubbs RR, Ferrario CM, Novick AC. Angiotensin II receptor subtypes in the human renal cortex and renal cell carcinoma. *J Urol* 1994;151:208-213.

19. Danser AH, van Kats JP, Admiraal PJ, Derkx FH, Lamers JM, Verdouw PD, Saxena PR, Schalekamp MA. Cardiac renin and angiotensins. Uptake from plasma versus in situ synthesis [see comments]. *Hypertension* 1994;24:37-48.

20. Lee KT. Swine as animal models in cardiovascular research. In: Tumbleson ME, ed. *Swine in biomedical research*. New York: Plenum Press; 1986:1481-1496.

21. Moulik S, Speth RC, Rowe BP. Differential loss in function of angiotensin II receptor subtypes during tissue storage. *Life Sci* 2000;66:L233-L237.

22. Corless CL, Kibel AS, Iliopoulos O, Kaelin WG. Immunostaining of the von Hippel-Lindau gene product in normal and neoplastic human tissues. *Hum Pathol* 1997;28:459-464.

23. Grone HJ, Simon M, Fuchs E. Autoradiographic characterization of angiotensin receptor subtypes in fetal and adult human kidney. *Am J Physiol* 1992;262:F326-F331.

24. Sechi LA, Grady EF, Griffin CA, Kalinyak JE, Schambelan M. Distribution of angiotensin II receptor subtypes in rat and human kidney. *Am J Physiol* 1992;262:F236-F240.

25. Mifune M, Sasamura H, Nakazato Y, Yamaji Y, Oshima N, Saruta T. Examination of angiotensin II type 1 and type 2 receptor expression in human kidneys by immunohistochemistry. *Clin Exp Hypertens* 2001;23:257-266.

26. Miyata N, Park F, Li XF, Cowley AW. Distribution of angiotensin AT1 and AT2 receptor subtypes in the rat kidney. *Am J Physiol* 1999;277:F437-F446.

27. Cao Z, Kelly DJ, Cox A, Casley D, Forbes JM, Martinello P, Dean R, Gilbert RE, Cooper ME. Angiotensin type 2 receptor is expressed in the adult rat kidney and promotes cellular proliferation and apoptosis [In Process Citation]. *Kidney Int* 2000;58:2437-2451.

28. Kakuchi J, Ichiki T, Kiyama S, Hogan BL, Fogo A, Inagami T, Ichikawa I. Developmental expression of renal angiotensin II receptor genes in the mouse. *Kidney Int* 1995;47:140-147.

29. Frid MG, Aldashev AA, Dempsey EC, Stenmark KR. Smooth muscle cells isolated from discrete compartments of the mature vascular media exhibit unique phenotypes and distinct growth capabilities. *Circ Res* 1997;81:940-952.

30. Frid MG, Dempsey EC, Durmowicz AG, Stenmark KR. Smooth muscle cell heterogeneity in pulmonary and systemic vessels. Importance in vascular disease. *Arterioscler Thromb Vasc Biol* 1997;17:1203-1209.

31. Hollenberg NK, Fisher ND, Price DA. Pathways for angiotensin II generation in intact human tissue: evidence from comparative pharmacological interruption of the renin system. *Hypertension* 1998;32:387-392.

32. Voors AA, Pinto YM, Buikema H, Urata H, Oosterga M, Rooks G, Grandjean JG, Ganten D, van Gilst WH. Dual pathway for angiotensin II formation in human internal mammary arteries. *Br J Pharmacol* 1998;125:1028-1032.

33. Lazard D, Briend-Sutren MM, Villageois P, Mattei MG, Strosberg AD. Molecular characterization and chromosome localization of a human angiotensin AT2 receptor gene highly expressed in tissues. *Receptors Channels* 1994;2:271-280.

FIGURE LEGENDS

Figure 1. AngII Receptors in Fetal Kidney. Representative autoradiographic images in ***Top Row*** show AT2R by *CGP binding (left-to-right): Total binding (AT2R+nonspecific); Nonspecific binding [*CGP + cold Sar^1AngII (S^1AII)]; AT2R [*CGP + Valsartan (Val), an AT1-selective analog]; and AT1R [*CGP + PD 123319 (PD), an unrelated AT2-selective compound used to confirm AT2R selectivity of CGP]. In ***Bottom Row***, *SIAII autoradiographic images reflect (left to right): Total ATR (AT1R+AT2R+non-specific); Nonspecific binding (*SIAII + cold S^1AII); AT2R (*SIAII + Val); and AT1R (*SIAII + PD). Each row represents a matched set of adjacent tissue sections. "Hot" refers to the relevant radioligand, "cold" to non-radioactive analogs.

Figure 2. Regional AngII Receptor Densities in Male vs Female Fetal Kidneys by Quantitative Image Analysis. Receptor densities, presented according to sex for indicated kidney regions, are shown for AT2R (left set of four paired bars) and AT1R (right paired bars). ***AT2R.*** AT2R density was high in all regions; the primordial medullary region significantly exceeded other regions ($p<.001$), which did not differ from each other. ***AT1R*** density was uniformly low ($\cong 1/40^{th}$ of AT2R density) and diffusely distributed. *Note differing Y axis scale for AT1R (right) cf AT2R (left).* There were no significant sex differences despite a trend toward higher AT2R and lower AT1R in females.

Figure 3. AngII Radioligand Binding in Fetal Kidney Membranes. Representative binding curves indicate: **A**. Specific **AT2R** Saturation Binding using AT2-selective

radioligand *CGP 42112. **B**. Specific **Total** (AT1R + AT2R) Saturation Binding via nonselective radioligand *SIAII; **C. Competition** Binding Curves using 0.55 nM *SIAII displaced by increasing concentrations of Valsartan (AT1-selective), CGP 42112 (AT2-Selective), or AngII (nonselective). **D**. **AT1R Binding**. Direct confirmation of AT1R using *SIAII saturation binding in the presence of 10^{-5}M cold CGP42112. Collectively, results show overwhelming dominance of AT2R in 90-Day fetal kidney. Results shown are representative of 14 experiments summarized in Table 1.

Figure 4. AngII Receptors in Neonatal Kidney by Autoradiography. Images are labeled as described for Figure 1. ***AT2R*** (Top Row, 1st and 3rd panels) are prominent in cortex as discrete AT2R-dense structures ("HotSpots") with variable shapes; there are no detectable AT2Rs in the intervening cortical tissue (see also FIG 7). AT2R were also present in outer medulla, papilla, and pelvic wall***. AT1R*** (Bottom Row, Righthand Panel) cortical binding shows discrete, intensely-AT1R-positive "hot dots" (glomerular profiles, see FIG 7) superimposed on less dense, homogenous extra-glomerular and medullary AT1R binding. AT1R was not visible in pelvic walls.

Figure 5. Regional AngII Receptor Densities in Neonatal Kidney by Quantitative Image Analysis. Autoradiographic receptor densities for indicated regions of the kidney are shown for AT2R (Left set of 6 bars) and AT1R (Right set of 6 bars). ***AT2R*-**rich cortical hotspots were of similar density in subcapsular vs main cortex and significantly greater than in the intervening ("background") cortical tissue (undetectable) and in the outer medullary region and papillary areas ($p<.001$ overall region effect). Pelvic-wall

AT2R density was high and similar to that of cortical Hotspots. ***AT1R*** density in glomerular profiles was similar in subcapsular vs main cortical regions and was significantly higher than that in extra-glomerular (background) cortical, medullary, or papillary regions. AT1R was undetectable in the pelvic wall.

Figure 6. AngII Receptor Distribution Patterns in Neonatal Kidney Cortex by Image Analysis. Data are shown for **AT2R (left-hand side)** and **AT1R (right-hand side)** and plotted separately for subcapsular cortex (hatched bars) vs main cortex (open bars) (See also Table 2). ***AT2Rs*** in cortex were present only *within* hotspots. The visual appearance of more confluent AT2R in the subcapsular vs main cortex region (eg FIG 4, Top left panel) was corroborated by significant increases in AT2R fractional area and number of hot spots/unit area without a size difference as compared to main cortex. ***AT1R*** distribution pattern (Right side) was notable for a 6-fold higher fractional area occupied by glomerular profiles in subcapsular (nephrogenic) cortex vs main cortex. However, the apparent increase in size and fractional area of glomerular profiles is overestimated, while glomerular density is underestimated: high density of normally-sized glomerular profiles led to merging of some outlines during image analysis.

Figure 7. Microscopic AngII Binding Sites in Neonatal Kidney. Adjacent kidney sections were autoradiographically processed for AT2R (middle left panel) or AT1R (middle right panel) binding or were immunochemically stained for Factor-VIII-related antigen [brown staining marks endothelial cells of glomerular tufts (***GI***) and vasculature] (Top panels). The most intense (but not all) ATR-positive sites in each autoradiogram

were captured by setting a density threshold, then overlaid on the matched, identically sized immunostained image (Lower panels). **AT2R binding sites** (Left Panels) were associated with intra-cortical and medullary microvessels (***Mv***), with juxta-glomerular (but not intra-glomerular) structures, and with nerves (***Nv***) accompanying pelvic arteries/veins. **AT1R binding sites** (Right panels) were maximally dense within glomerular tufts. All extraglomerular structures were homogenously positive for AT1R at a lower density, including tubules and microvessels.

Figure 8. AngII Receptors in Adult Kidney by Autoradiography. Images are labelled as described for Fig 1. ***AT2R*** (Top Row) in cortex were distributed in a magnified version of the neonatal pattern – discrete hotspots with no detectable specific binding in intervening tissue. Dense binding in a large preglomerular penetrating artery is visible at the cortico-medullary junction. However, unlike neonates, there was no AT2R binding in the outer medulla or papilla of the adult kidney. ***AT1R*** (Bottom Row, right hand image) again exhibits a pattern of maximally dense glomerular profiles superimposed on diffuse extraglomerular AT1R binding of lower density, prominently including the outer medullary stripe. There was no distinguishable subcapsular cortical region in adult kidneys. When present in autoradiographs, pelvic wall was consistently AT2R positive (not shown).

Figure 9. Regional AngII Receptor Densities in Adult Kidney by Quantitative Image Analysis. AT2R density is shown in the left set of bars, AT1R in the right set of bars. **AT2R** binding was high in cortical Hotspots and undetectable in intervening

cortical tissue and medulla. **AT1R** density of adult glomerular profiles was statistically similar to neonatal levels and exceeded both the diffuse extraglomerular cortical and the outer medullary AT1R densities in the adult kidney.

Figure 10. AngII Radioligand Binding Adult Kidney Membranes. A. Representative *SIAII saturation binding curve indicates total AngII receptors in adult kidneys. Bmax is 100-fold lower than that of fetal kidneys in Fig 3. *CGP binding was undetectable in 8 of 8 adult kidneys (data not shown), indicating AT2 receptors are below assay sensitivity in the whole-kidney preparation. **B. Competition Binding Curves** using 0.55 nM *SIAII displaced by analogs Valsartan (AT1-Selective), CGP 42112 (AT2 Selective), or AngII (nonselective) shows virtually 100% AT1R here; AT2R ranged 0 - 30%.

Figure 11. AngII Receptors in Normal Adult Rat Kidney by Autoradiography. Because of discrepancy among published reports, we examined three adult rat kidneys for AT1R (Left Panels) and AT2R (Right Panels) by autoradiographic methods identical to those applied to microswine kidneys reported here. After 24 hrs exposure, AT2R binding by *CGP autoradiography was undetectable, whereas AT1R binding using *SIAII + CGP autoradiography was abundant.

Table 1

Ang II Receptor Binding in Fetal Kidney Membranes*

	Male	Female	p value
Total ATR (Bmax *SIAII)	272 ± 214	459 ± 331	NS
Total AT2R (Bmax *CGP)	324 ± 244	379 ± 240	NS
% AT2R†	96 ± 3	96 ± 3	NS
% AT1R‡	4 ± 3	4 ± 3	NS
Kd *SIAII	0.27 ± 0.18	0.77 ± 0.51	< .025
Kd *CGP	0.05 ± 0.03	0.13 ± 0.09	< .035
Ang II Log IC_{50}	-8.76 ± 0.27	-9.03 ± 0.74	NS
CGP 42112 Log IC_{50}	-9.47 ± 0.60	-9.53 ± 0.55	NS
(n)	(8)	(6)	

* Receptor number expressed as fmol ligand bound/mg protein; *SIAII - ^{125}I-Sar^{1}Ile^{8}AngII; *CGP - ^{125}I-CGP 42112; Bmax - maximum binding at saturating radioligand concentration; Kd - dissociation constant (nM); Log IC_{50} – $\log_{10}$ concentration (nM) of competing analog at 50% radioligand displacement; n – no. of animals studied.

† %AT1R based on displacement by Valsartan

‡ %AT2R based on displacement by CGP 42112

Table 2.

Ang II Receptors in Neonatal vs Adult Kidney Cortex

by Quantitative Autoradiography*

	AT1 Receptors		AT2 Receptors
	Glomerular Profiles	**Extra-Glomerular Cortex**	**Cortical "Hotspots"†**
Neonatal Cortex*			
ATR Density*	1549 ± 376	856 ± 459	2818 ± 453
Fxl Area (%)‡	3 ± 2	---	6 ± 2
Size (Pixels)	8 ± 4	---	15 ± 5
#/kpxl§	4 ± 1	---	4 ± 1
(n)	(5)	(5)	(5)
Adult Cortex*			
ATR Density	1041 ± 646	351 ± 243	777 ± 280
Fxl Area (%)‡	10 ± 5	---	8 ± 5
Size (Pixels)	30 ± 9	---	33 ± 13
#/kpxl§	3 ± 1	---	2 ± 0
(n)	(5)	(5)	(5)
p Age Effect			
ATR Density	NS	NS	<.0001
Fxl Area‡	<.04		NS
Size	<.001		<.05
#/kpxl§	NS		<.01

*ATR density expressed in fmol/gm (mean ± SD): ^{125}I-CGP 42112A (for AT2R) or ^{125}I-SIAII + cold CGP 42112 (for AT1R). Adult values are compared to those of the main (not subcapsular) cortex in neonates.

† AT2R "Hotspots" indicates AT2R-dense structures in postnatal kidney cortex, largely reflecting microvessels

‡ Fxl Area: % of cortical cross-sectional area occupied by AT2R Hotspots or by AT1R-rich glomerular profiles.

§ #/kpxl : number of receptor-rich structures (glomeruli profiles for AT1R, "Hotspots" for AT2R) per kilopixel of cortical cross-sectional area

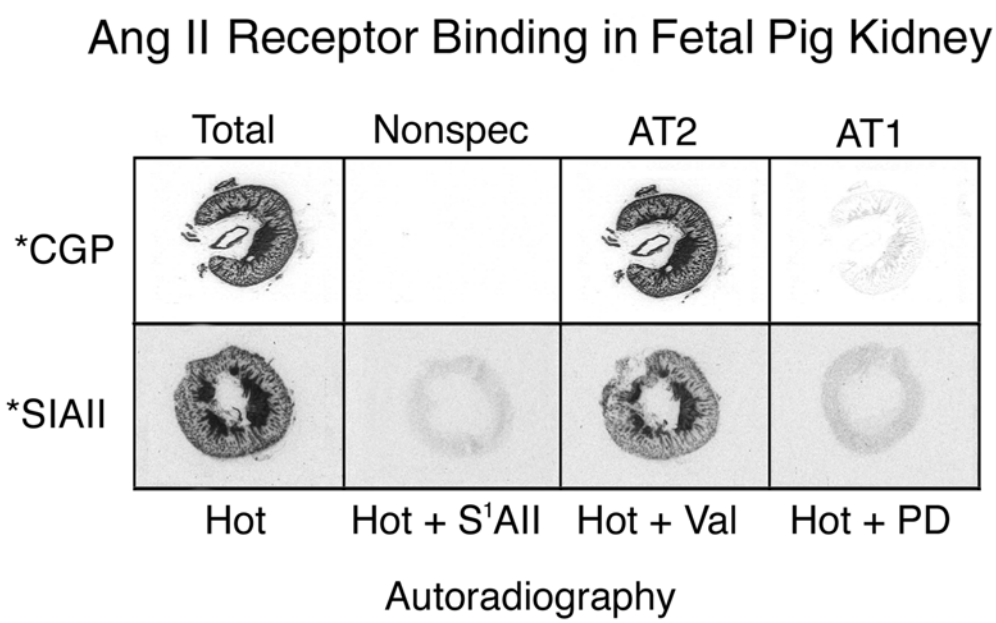
Ang II Receptor Binding in Fetal Pig Kidney
Total
Nonspec
AT2
AT1
*CGP
*SIAII
Hot
Hot + S1AII
Hot + Val
Hot + PD
Autoradiography

FIGURE 1

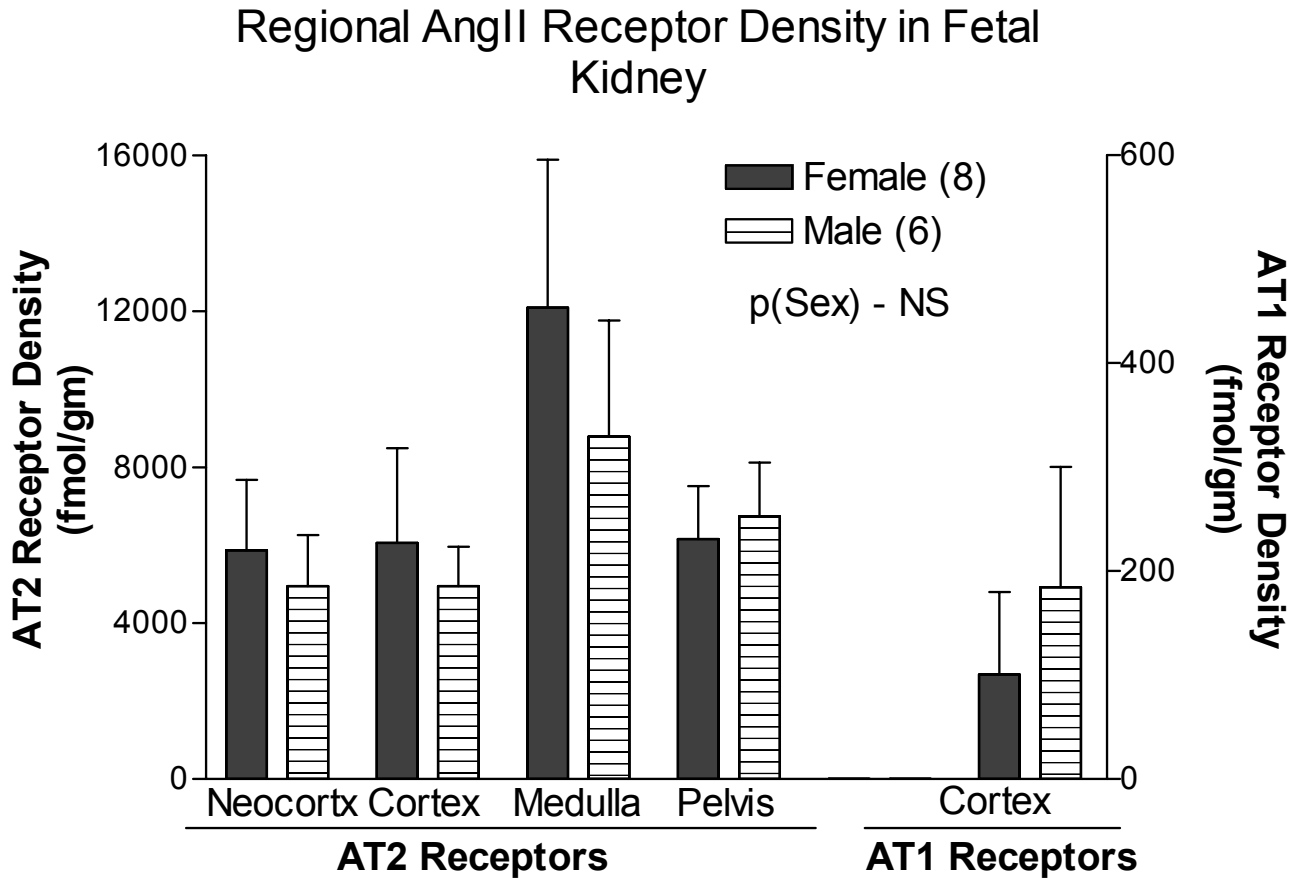
Regional AngII Receptor Density in Fetal Kidney
AT2 Receptor Density (fmol/gm)
AT1 Receptor Density (fmol/gm)
16000
12000
8000
4000
0
600
400
200
0
Female (8)
Male (6)
p(Sex) - NS
Neocortx
Cortex
Medulla
Pelvis
Cortex
AT2 Receptors
AT1 Receptors

FIGURE 2

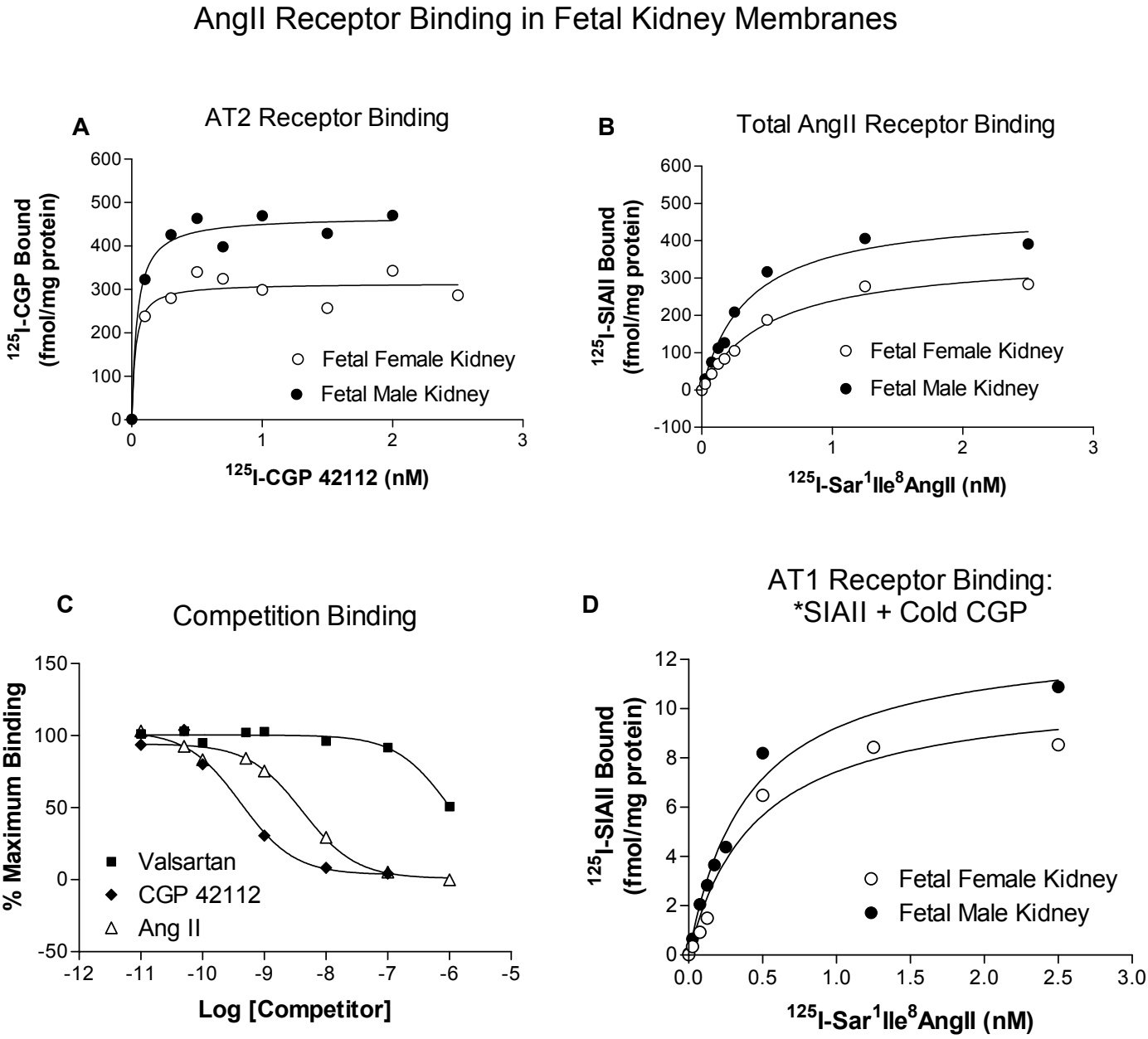
AngII Receptor Binding in Fetal Kidney Membranes
A
AT2 Receptor Binding
125I-CGP Bound (fmol/mg protein)
125I-CGP 42112 (nM)
Fetal Female Kidney
Fetal Male Kidney
B
Total AngII Receptor Binding
125I-SIAII Bound (fmol/mg protein)
125I-Sar1Ile8AngII (nM)
Fetal Female Kidney
Fetal Male Kidney
C
Competition Binding
% Maximum Binding
Log [Competitor]
Valsartan
CGP 42112
Ang II
D
AT1 Receptor Binding:
*SIAII + Cold CGP
125I-SIAII Bound (fmol/mg protein)
125I-Sar1Ile8AngII (nM)
Fetal Female Kidney
Fetal Male Kidney

FIGURE 3

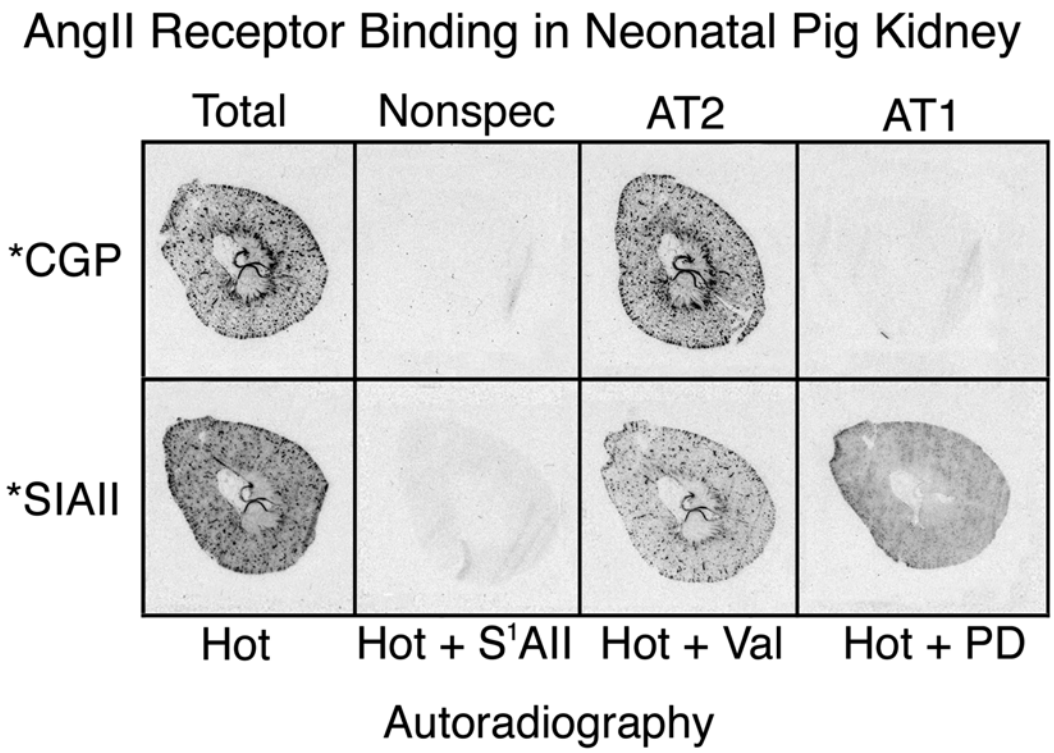
AngII Receptor Binding in Neonatal Pig Kidney
Total
Nonspec
AT2
AT1
*CGP
*SIAII
Hot
Hot + S1AII
Hot + Val
Hot + PD
Autoradiography

FIGURE 4

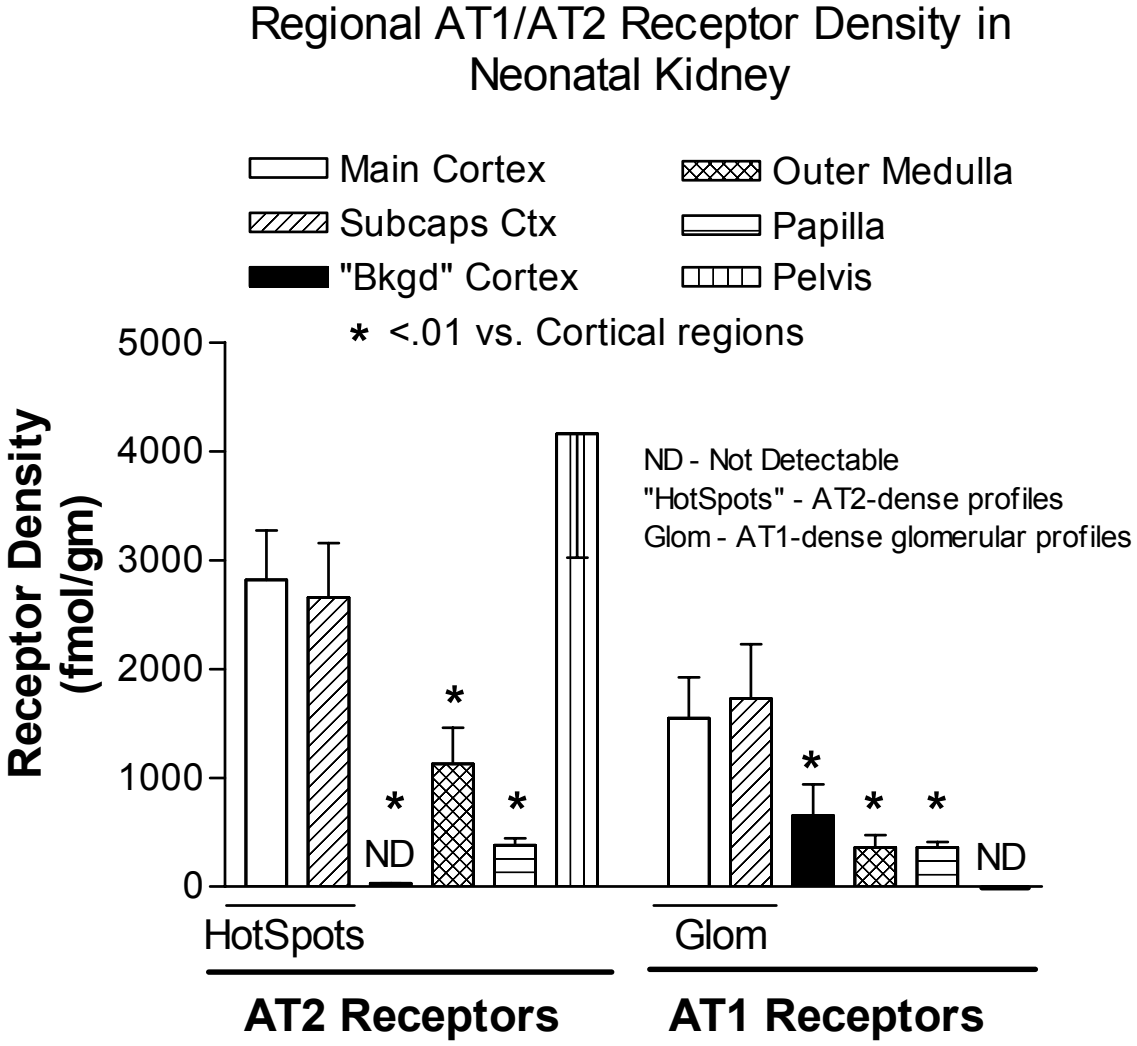
Regional AT1/AT2 Receptor Density in Neonatal Kidney
Main Cortex
Outer Medulla
Subcaps Ctx
Papilla
"Bkgd" Cortex
Pelvis
* <.01 vs. Cortical regions
Receptor Density (fmol/gm)
5000
4000
3000
2000
1000
0
ND - Not Detectable
"HotSpots" - AT2-dense profiles
Glom - AT1-dense glomerular profiles
ND
ND
HotSpots
Glom
AT2 Receptors
AT1 Receptors

FIGURE 5

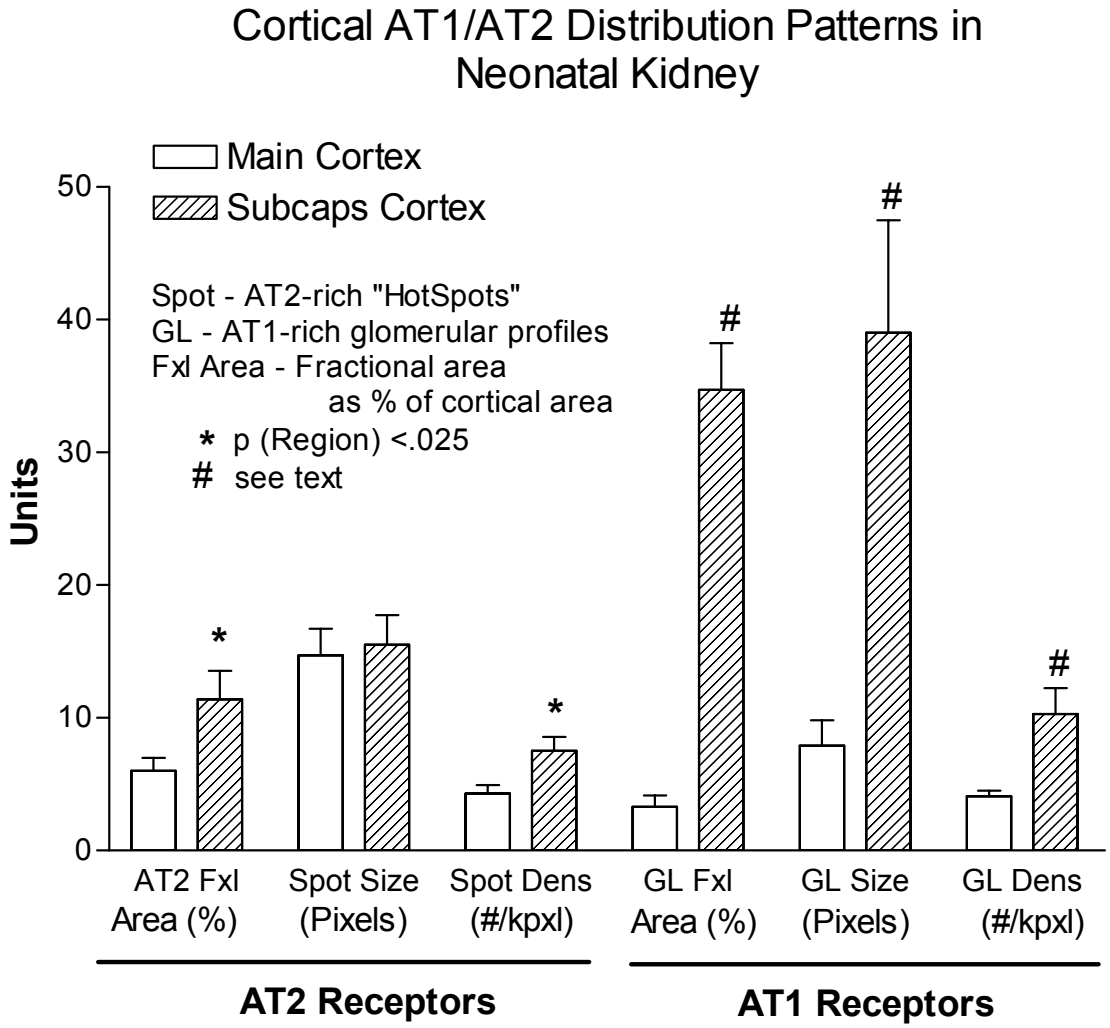
Cortical AT1/AT2 Distribution Patterns in Neonatal Kidney
Main Cortex
Subcaps Cortex
Spot - AT2-rich "HotSpots"
GL - AT1-rich glomerular profiles
Fxl Area - Fractional area as % of cortical area
* p (Region) <.025
# see text
Units
50
40
30
20
10
0
*
*
#
#
#
AT2 Fxl Area (%)
Spot Size (Pixels)
Spot Dens (#/kpxl)
GL Fxl Area (%)
GL Size (Pixels)
GL Dens (#/kpxl)
AT2 Receptors
AT1 Receptors

FIGURE 6

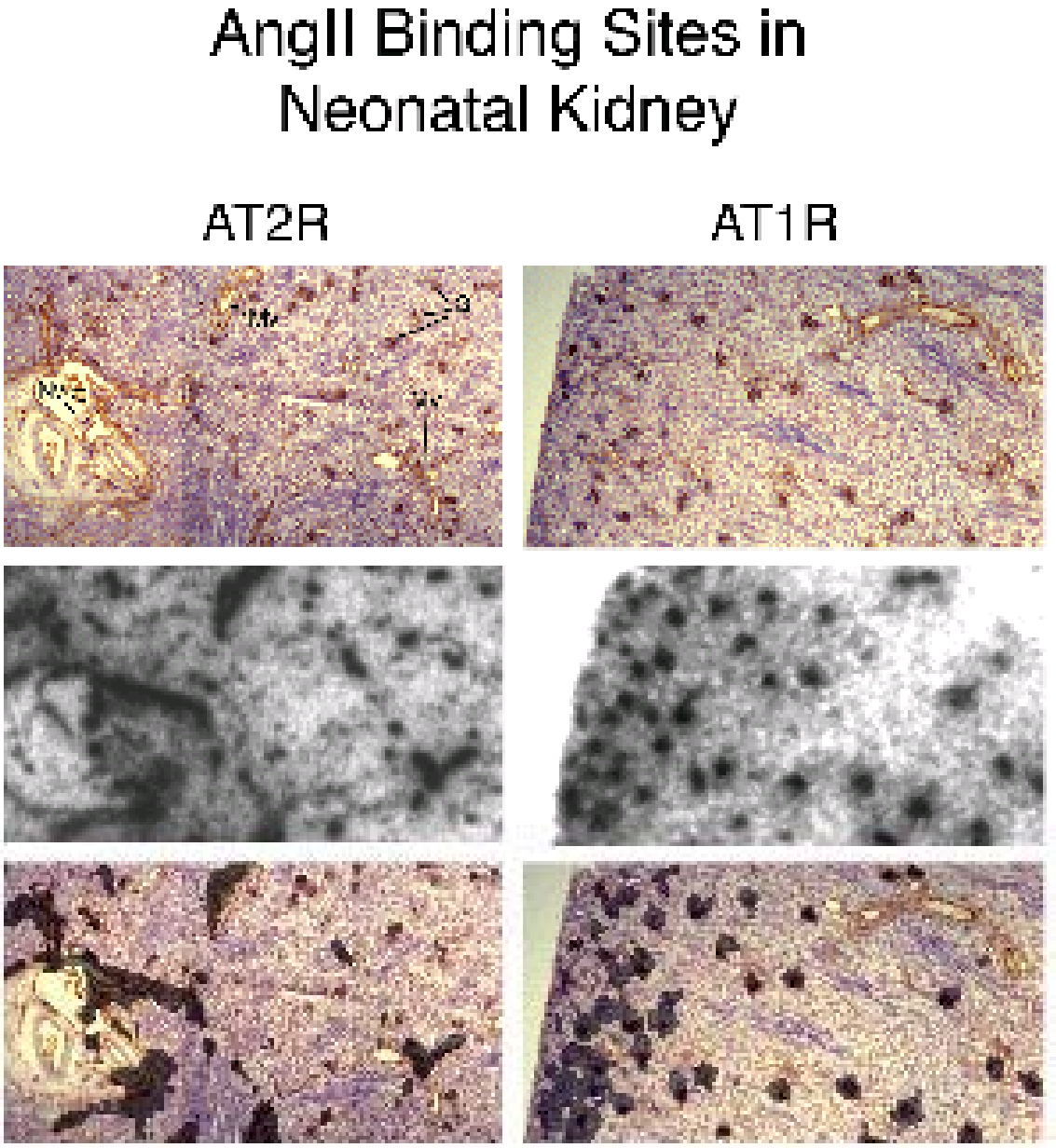

FIGURE 7

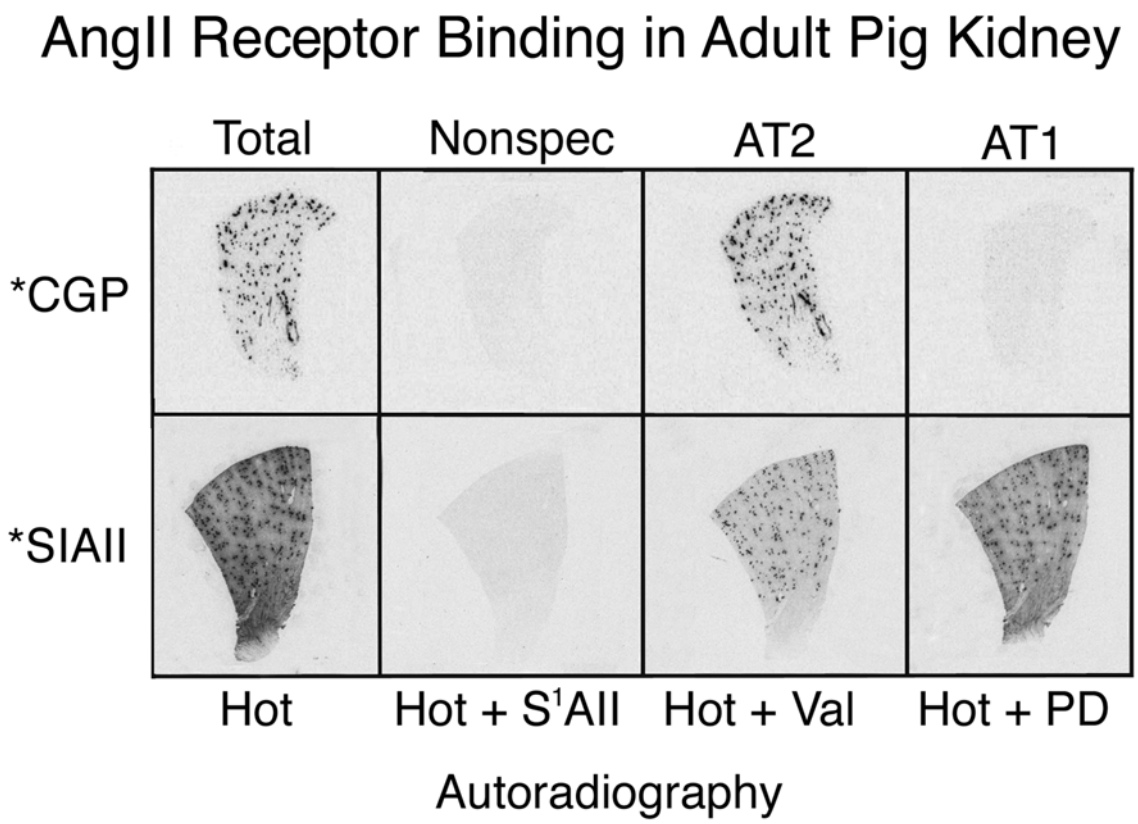
AngII Receptor Binding in Adult Pig Kidney
Total
Nonspec
AT2
AT1
*CGP
*SIAII
Hot
Hot + S1AII
Hot + Val
Hot + PD
Autoradiography

FIGURE 8

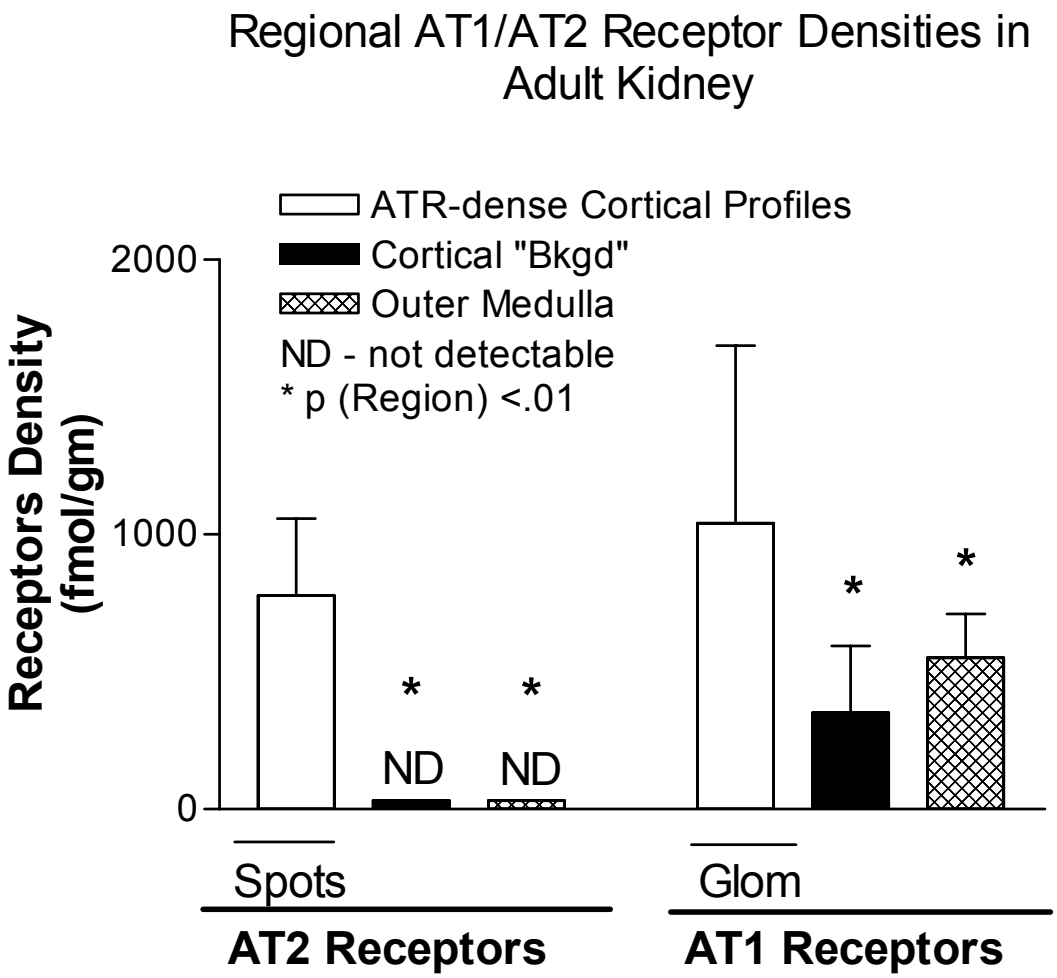
Regional AT1/AT2 Receptor Densities in Adult Kidney
ATR-dense Cortical Profiles
Cortical "Bkgd"
Outer Medulla
ND - not detectable
* p (Region) <.01
Receptors Density (fmol/gm)
2000
1000
0
*
*
ND
ND
*
*
Spots
Glom
AT2 Receptors
AT1 Receptors

FIGURE 9

AngII Receptor Binding in Adult Kidney Membranes

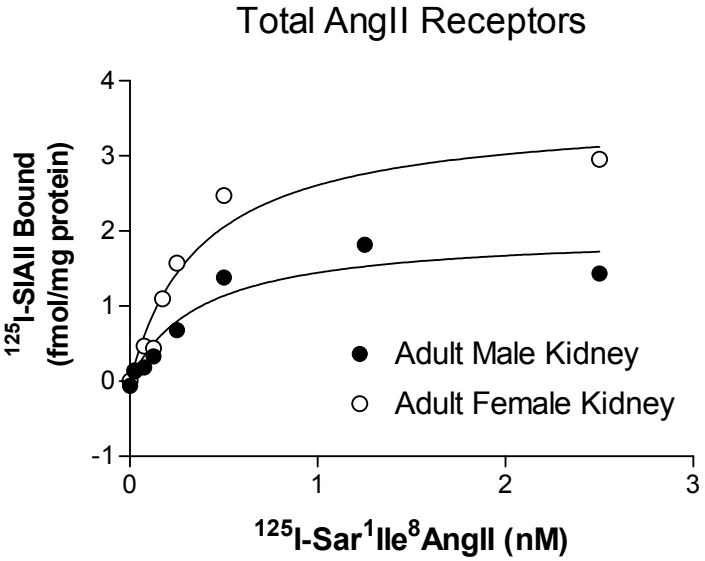

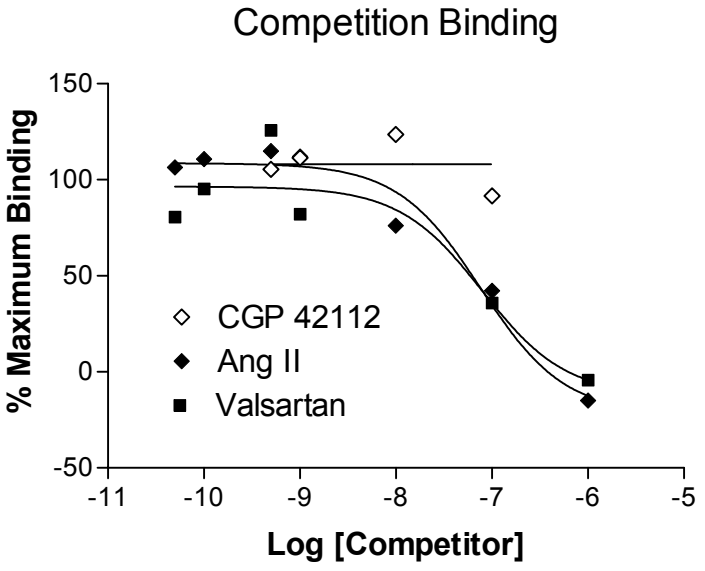

FIGURE 10

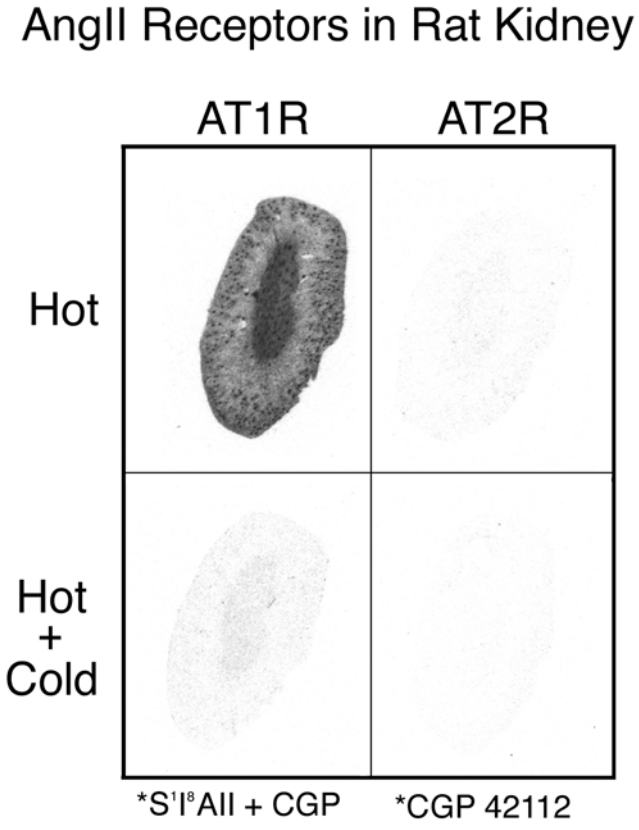
AngII Receptors in Rat Kidney
AT1R
AT2R
Hot
Hot
+
Cold
*S¹I⁸AII + CGP
*CGP 42112

FIGURE 11